Allosteric Inhibition of Zinc-Finger Binding in the Major Groove of DNA by Minor-Groove Binding Ligands†

Doan H. Nguyen-Hackley,‖,⊥ Elizabeth Ramm,‡,⊥ Christina M. Taylor,§ J. Keith Joung,§ Peter B. Dervan,*,‖ and Carl O. Pabo‡

Howard Hughes Medical Institute and Department of Biology, Massachusetts Institute of Technology, Cambridge, Massachusetts 02139, and Division of Chemistry and Chemical Engineering, California Institute of Technology, Pasadena, California 91125

Received October 15, 2003; Revised Manuscript Received January 14, 2004

ABSTRACT: In recent years, two methods have been developed that may eventually allow the targeted regulation of a broad repertoire of genes. The engineered protein strategy involves selecting Cys_2His_2 zinc finger proteins that will recognize specific sites in the major groove of DNA. The small molecule approach utilizes pairing rules for pyrrole−imidazole polyamides that target specific sites in the minor groove. To understand how these two methods might complement each other, we have begun exploring how polyamides and zinc fingers interact when they bind the same site on opposite grooves of DNA. Although structural comparisons show no obvious source of van der Waals collisions, we have found a significant "negative cooperativity" when the two classes of compounds are directed to the overlapping sites. Examining available crystal structures suggests that this may reflect differences in the precise DNA conformation, especially with regard to width and depth of the grooves, that is preferred for binding. These results may give new insights into the structural requirements for zinc finger and polyamide binding and may eventually lead to the development of even more powerful and flexible schemes for regulating gene expression.

Recent developments in the design and selection of Cys_2His_2 zinc fingers (*1*, *2*) and in the design of novel polyamides (*3*, *4*) suggest that each method can be used to target specific sites in the genome. Cys_2His_2 zinc finger proteins, in which each domain contains 28−30 amino acid residues, are the most common DNA-binding motif in higher eukaryotes. Each zinc finger has a conserved $\beta\beta\alpha$ motif, and amino acids near the N-terminus of the α-helix contact bases in the major groove of B-DNA (*2*, *5*−*7*). The X-ray crystal structure of the three-finger Zif268 protein (Figure 1A, refs *6*, *7*) illustrates the basic features of recognition and has provided the basis for most of the subsequent work in this field. The Cys_2His_2 zinc finger framework appears to be very adaptable, and specific variants have been selected that bind to many different desired target sites in duplex DNA (*8*−*11*).

Another strategy for recognition and regulation has been developed that uses polyamides consisting of *N*-methylpyrrole (Py)[1] and *N*-methylimidazole (Im) rings, which can be linked together to recognize a predetermined DNA sequence (*3*, *4*). Sequence-specific polyamide−DNA recognition depends on binding in the minor groove with side-by-side amino acid pairings. Simple rules were developed for designing polyamides that can target desired DNA sequences (*4*). These rules have been carefully validated through characterization of synthesized polyamides via DNase I footprinting, affinity cleavage, two-dimensional nuclear magnetic resonance (NMR) (*12*), and X-ray crystallographic methods (*13*−*15*). To illustrate the docking arrangement, Figure 1B shows the X-ray crystal structure of a polyamide (*15*) bound in the minor groove of B-DNA.

In this work, we have begun studies to investigate how polyamides and zinc fingers may interact as they bind to overlapping sites on double-stranded DNA. Earlier studies have explored how polyamides interfere with the binding of several classes of transcription factors (*16*−*23*). Polyamides have inhibited minor-groove binding proteins such as TATA-binding protein (TBP), as well as minor groove contacting proteins like the lymphoid enhancer factor (LEF-1) (*17*). In the case of the purely major-groove binding protein GCN4, polyamides were clearly shown to co-occupy in the minor groove of the GCN4 binding site (*21*). An extended Arg-Pro-Arg tripeptide attached to a polyamide did inhibit GCN4 binding by neutralizing a phosphate contact made by the protein with the DNA backbone (*22*). Polyamides have been

† C.M.T. was supported by a NSF predoctoral fellowship, J.K.J. was supported by a HHMI Physician Postdoctoral Fellowship, E.R. and C.O.P. were supported by the Howard Hughes Medical Institute, D.H.N. was supported by a Natural Sciences and Engineering Research Council of Canada Postgraduate Scholarship, and P.B.D. was supported by NIH Grant GM 51747.

* To whom correspondence should be addressed.

‖ California Institute of Technology.

⊥ These authors contributed equally to this work.

‡ Howard Hughes Medical Institute, Massachusetts Institute of Technology.

§ Department of Biology, Massachusetts Institute of Technology.

[1] Abbreviations: NMR, nuclear magnetic resonance; Py, *N*-methylpyrrole; Im, *N*-methylimidazole; PA, polyamide; $TATA_{ZF}$, Zif268 variant that recognizes the TATA binding site; NRE_{ZF}, Zif268 variant that recognizes the NRE binding site; $p53_{ZF}$, Zif268 variant that recognizes the p53 binding site; DTT, dithiolthreitol; TFA, trifluoroacetic acid; ACN, acetonitrile.

10.1021/bi030223c CCC: $27.50
Published on Web 03/13/2004

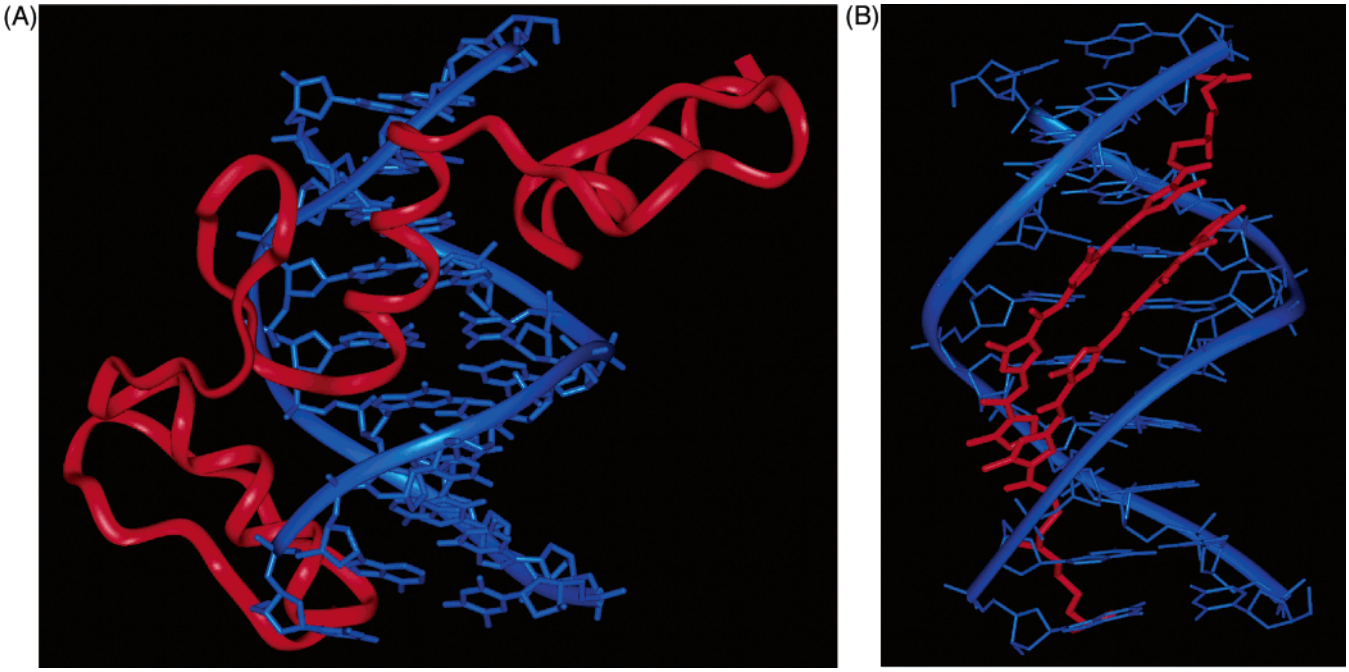

FIGURE 1: (A) Crystal structure of the Zif268 zinc finger protein (red, with ribbon representing protein backbone) bound in the major groove of B-DNA (blue, with ribbon connecting phosphates) [coordinates are from ref 6] anc (B) crystal structure of a polyamide (red) bound in minor groove of B-DNA (blue) [coordinates are from ref 15, 1CVY].

shown to inhibit the binding of a zinc finger protein, TFIIIA (*16*, *20*). However, inhibition of this zinc finger protein was the result of the polyamide being targeted to and displacing the minor-groove-spanning fourth finger of the nine-finger protein. Therefore, studies to date on polyamide/protein interactions would suggest that an unmodified polyamide should co-occupy the minor groove face of a purely major groove zinc finger protein binding site.

In this study, the interaction of polyamides and zinc fingers that bind to opposing grooves of the same DNA target site was explored. The zinc finger proteins chosen for this study included Zif268 and a set of Zif268 variants that had been selected to recognize rather different DNA sequences (*9*). These three other variants had been selected to recognize the TATA box, the nuclear receptor element, and the p53 binding sites, and they are referred to (respectively) as $TATA_{ZF}$, NRE_{ZF}, and $p53_{ZF}$. All these proteins bind their sites with nanomolar dissociation constants, recognizing sites in the DNA major groove and discriminating effectively against nonspecific DNA (*9*, *24*). For this project, polyamides **1**−**4** were designed to specifically target the very same TATA, NRE, p53, and Zif268 binding sites. These hairpin polyamides bind their sites with at least nanomolar dissociation constants, as determined by quantitative DNase I footprinting experiments (*25*−*28*). Biochemical studies, using gel mobility shift experiments and DNase I analysis, give information about how these compounds interact as they bind. Computer modeling based on previous structural studies of zinc finger−DNA and polyamide−DNA complexes help us to interpret these results.

MATERIALS AND METHODS

Protein Production and Purification. The Zif268 zinc finger region (residues 333−421) was subcloned into a pET-21d expression vector (Novagen) and was transformed into the *Escherichia coli* strain BL21(DE3) containing the pLysE plasmid. Cultures were grown and induced as described (Novagen). After the cells were harvested, they were lysed and sonicated as recommended (Novagen). The peptides were denatured and reduced in 6.4 M guanidine·HCl, 150 mM DTT, and 50 mM Tris-HCl, pH 8.0, at 75 °C for 30 min and acidified to pH ≈ 2.0 by addition of 10% trifluoroacetic acid (TFA). The peptides were purified by reverse-phase batch extraction on Sep-pack C-18 cartridges (Waters) as described (*29*), followed by purification on a C4 reversed-phase (Vydac) high-performance liquid chromatography column using a gradient of 22−35% acetonitrile (ACN) containing 0.1% TFA. The purified peptide fractions were then refolded anaerobically in the binding buffer that we used for gel shifts, after supplementing it with a 0.5 M excess of $ZnCl_2$. Refolded peptides were stored at −80 °C in 10 μL aliquots; each aliquot was used once for binding studies and then discarded. The active concentrations of peptides were determined in stoichiometric competition experiments.

$TATA_{ZF}$, NRE_{ZF}, and $p53_{ZF}$ zinc finger peptides, selected from residues 333−421 of Zif268 (*24*), used in these studies were purified by Scot A. Wolfe, Robert Grant, and Sandra Fay-Richard, respectively. Since they were preparing these samples for crystallographic studies, they used several additional purification steps, essentially as described (*30*).

Hairpin Polyamide Syntheses and Characterization. The pyrrole−imidazole hairpin polyamides **1**−**4** were prepared by manual and machine-assisted solid-phase methods (*31*) (Figures 2 and 3). Purity and identity of each compound were verified by a combination of analytical HPLC, ^{1}H NMR, and matrix-assisted laser desorption ionization time-of-flight mass spectrometry (MALDI-TOF). Polyamides **1**−**3** have been described previously (*32*, *33*) and polyamide **4**, PyIm-β-Im-$(R)^{H}2^{N}\gamma$-PyImPyPy-β-Dp, is described here: UV (H_2O) λ_{max}-304 (60 800); MALDI-TOF MS 1230.65 (1230.59 calcd for $[M + H]$ $C_{55}H_{72}N_{23}O_{11}^{+}$). Lyophilized samples of polyamides were stored in at −80 °C. Polyamide concentrations were

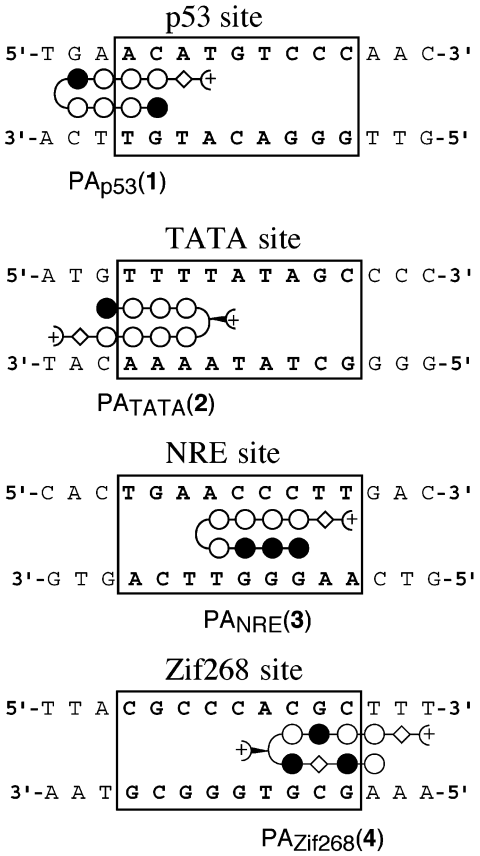

FIGURE 2: Minor-groove binding models expected for hairpin complexes of ImPyPyPy-γ-ImPyPyPy-β-Dp (**1**, PA_{p53}), ImPyPyPy-$(R)^H2^N\gamma$-PyPyPyPy-β-Dp (**2**, PA_{TATA}), ImImImPy-γ-PyPyPyPy-β-Dp (**3**, PA_{NRE}), and ImPyPyPy-$(R)^H2^N\gamma$-PyPyPyPy-β-Dp (**4**, PA_{Zif268}) targeted to their match sites in the minor groove opposite the $p53_{ZF}$, $TATA_{ZF}$, NRE_{ZF}, and $Zif268_{ZF}$ major-groove binding sites. Shaded and unshaded circles represent imidazole and pyrrole carboxamides, respectively, and the β-alanine residue is represented by an unshaded diamond. Boxes enclose the nine base pair sites that are recognized by the corresponding zinc finger proteins.

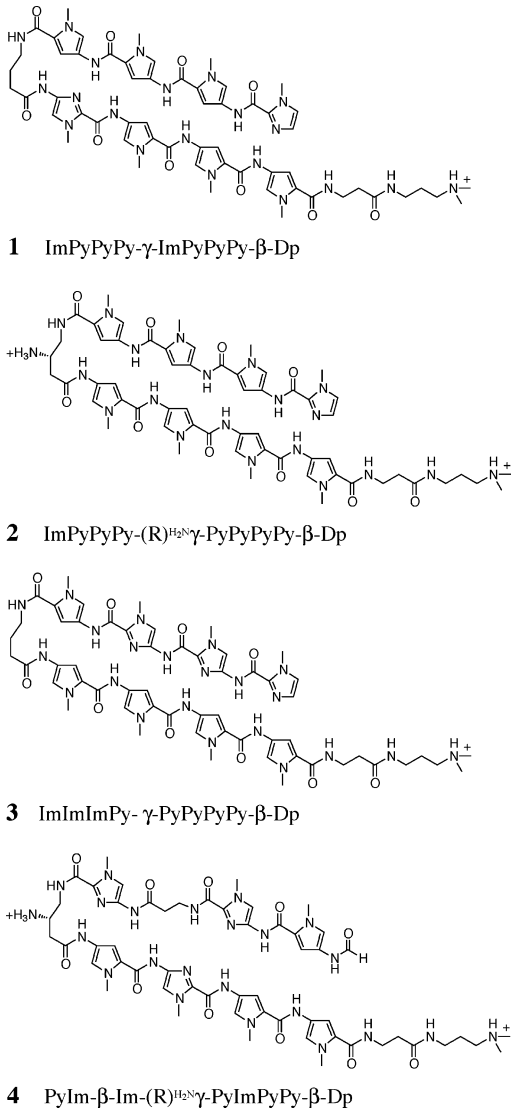

FIGURE 3: Full chemical structures of the hairpin polyamides: PA_{p53}, ImPyPyPy-γ-ImPyPyPy-β-Dp (**1**), PA_{TATA}, ImPyPyPy-$(R)^H2^N\gamma$-PyPyPyPy-β-Dp (**2**), PA_{NRE}, ImImImPy-γ-PyPyPyPy-β-Dp (**3**), and PA_{Zif268}, ImPyPyPy-$(R)^H2^N\gamma$-PyPyPyPy-β-Dp (**4**).

determined spectrophotometrically with extinction coefficients estimated based on the number of aromatic rings using the relation 8690 M^{-1} cm^{-1} per aromatic ring for the absorption maximum at 290−315 nM (*28*).

Gel Mobility Shift Assay. Double-stranded oligonucleotides used for gel mobility shift assays were essentially identical to DNA sites used (*9*) when selecting the $TATA_{ZF}$, NRE_{ZF}, and $p53_{ZF}$ zinc finger proteins. A few nucleotides in the sequence flanking the zinc finger binding sites also were changed so that the zinc fingers and polyamides would have overlapping binding sites. The 27 bp DNA duplexes that were used for gel mobility shift assays are boxed in Figure 4, and the nine base pair zinc finger target sites near the center of each duplex are underlined. (Note that in the form shown in Figure 4, 27 bp duplexes are embedded within larger DNA segments that were later used for footprinting studies.) The oligonucleotide binding site for wt Zif268 was slightly different from that used by Greisman et al. (*9*) containing GCGGGGGCG rather than GCGTGGGCG. However, this construct was advantageous because it readily provided an overlapping polyamide binding site and should have no other effect. (Zif268 binds extremely well to either site and there is no direct contact with this base in the crystal structure (*6*)).

Each 27 bp strand of these binding sites was synthesized using standard phosphoramidite chemistry on an Applied Biosystems model 392 DNA synthesizer. Following deprotection, oligonucleotides were purified by denaturing polyacrylamide gel electrophoresis. Duplexes were annealed and quantified, and then 0.3 pmol of each DNA fragment were end-labeled with [α-^{32}P]-ATP (New England Biolabs) using Klenow exo$^-$ to fill-in the overhangs. Unincorporated nucleotides were removed by use of Sephadex G-25 quick spin columns (Boehringer Mannheim), and the DNA was resuspended in 1 mL of the buffer used for all gel shift experiments, which contained 5 mM HEPES, pH 7.8, 50 mM KCl, 50 mM KGlu, 50 uM KoAc, 5 mM $MgCl_2$, 5% glycerol, 0.1% NP-40, 20 uM $ZnSO_4$, 100 ug/mL BSA, 1 mM $CaCl_2$, and 1 mM DTT. The nucleotides were stored at −20 °C.

Using the buffer above, we performed binding reactions and equilibrium binding studies for zinc finger proteins in both the presence and absence of polyamides. Zinc finger dissociation constants were determined as previously described (*9*), except that 0.5 pM of labeled duplex DNA was

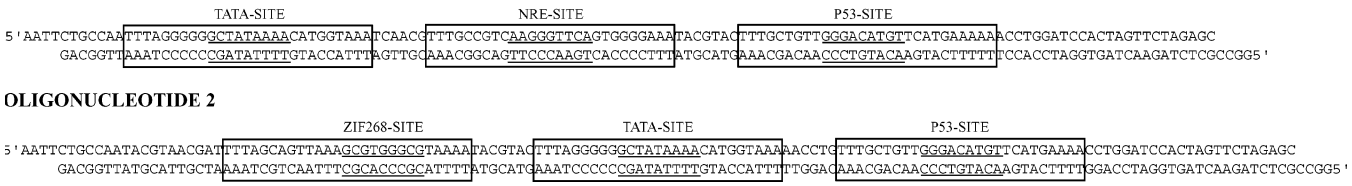

FIGURE 4: Oligonucleotide sequences used for DNase I footprinting experiments, with each of the nine base pair target sites for the zinc finger proteins underlined. Oligonucleotide 1 contains the $TATA_{ZF}$, NRE_{ZF}, and $p53_{ZF}$ binding sites; oligonucleotide 2 contains the Zif268, $TATA_{ZF}$, and $p53_{ZF}$ binding sites. Gel mobility assays used shorter oligonucleotides (27 bp segments each containing a single binding site), and the corresponding segments used in these experiments are shown as boxed regions surrounding each of the nine base pair binding sites. In this orientation, the site that has been cleaved by *Eco*RI is at the left end of the oligonucleotide; the site cleaved by *Not*I is on the right.

used and equilibration was done at room temperature for 16−18 h for all gel shift experiments. The reaction mixtures were then subjected to 12% native polyacrylamide gel electrophoresis for about 2 h with 0.5× TBE running buffer. Radioactive signals were quantitated by PhosphorImage analysis (Molecular Dynamics).

Equilibrium dissociation constants (K_D's) were determined by linear regression using the Scatchard equation:

$$\Theta/[P] = 1/K_D - \Theta/K_D \quad (1)$$

in which Θ equals the fraction of DNA bound ([PD]/([PD] + [D])), and [P] equals the free protein concentration (after applying corrections to account for the percent of the protein that was active for DNA binding).

DNase I Footprinting. Oligonucleotides used for footprinting experiments (Figure 4) were designed so that they included the sequences of the 27 bp duplexes that had been used for gel mobility shift assays, and additional six to seven base pair "spacers" were added so that the protein-binding sites would be slightly further apart. Oligonucleotide 1 contains binding sites for $TATA_{ZF}$, NRE_{ZF}, and $p53_{ZF}$; oligonucleotide 2 contains binding sites for Zif268, $TATA_{ZF}$, and $p53_{ZF}$. The synthetic duplexes were designed such that the ends were ready for cloning into a pBluescript II SK(+) plasmid (Stratagene) that had been cut with *Eco*RI and *Bam*HI. After growth in *E. coli*, DNA probes for footprinting were prepared by digestion of the appropriate plasmids with *Eco*RI and *Not*I restriction enzymes, giving a 134 bp fragment for oligonucleotide 1 and a 143 bp fragment for oligonucleotide 2. After digestion, these DNA fragments were radioactively labeled by using Klenow enzyme (New England Biolabs) and α-^{32}P labeled nucleotides to fill in the overhanging ends. The labeled oligonucleotides were purified using 5% native PAGE, were precipitated with EtOH, and were counted for specific activity.

Footprinting experiments were done essentially as previously described (*25*−*28*). Quantitative footprinting for polyamides **1**−**4** was performed using the appropriate restriction fragment (oligonucleotide 1 or 2) in triplicate under both conventional TKMC buffer (10 mM Tris-HCl (pH 7.0), 10 mM KCl, 10 mM $MgCl_2$, and 5 mM $CaCl_2$) and the same binding buffer used in the gel shift experiments. Polyamide/DNA solutions were allowed to equilibrate at 22 °C for 16−18 h. Footprinting reactions were initiated by the addition of the appropriate amount of DNase I to give ∼50% intact DNA and allowed to proceed for 7 min at 22 °C. The reactions were stopped by addition of 50 μL of a solution containing 1.25 M NaCl, 100 mM EDTA, 0.2 mg/mL glycogen, and 28 μM base-pair calf thymus DNA and ethanol precipitated. The reactions were resuspended in 1 μL of TBE/80% formamide loading buffer, denatured by heating at 80 °C for 10 min, and placed on ice. The reaction products were separated by electrophoresis. Radioactive signals were visualized with a Molecular Dynamics Typhoon phosphorimager followed by quantitation using ImageQuant software (Molecular Dynamics). Equilibrium association constants for the polyamides were calculated as previously described (*29*) and found to be identical in both TKMC buffer and the gel shift buffering conditions.

Computer Modeling Experiments. Structures of polyamide−DNA complexes were taken from the Protein Data Bank (*13*−*15*) and were compared with known zinc finger−DNA complexes for $TATA_{ZF}$ (*34*), $p53_{ZF}$ (*35*), and Zif268 (*6*). The structures were aligned (using the PROTEUS Program (*36*)) via phosphorus atoms, C1′ atoms, or common atoms in the set of superimposed base pairs. Several different alignment strategies were tested, including schemes in which (1) the entire zinc finger DNA binding site was aligned with the polyamide DNA, (2) the polyamide binding sites in the known polyamide−DNA structures were aligned with the expected polyamide binding sites on the zinc finger DNA, (3) the GC or AT base pair in the polyamide−DNA structure was aligned with the corresponding base pair in the DNA−zinc finger structure, or (4) all the common atoms in a base pair were aligned. The RMS deviation was noted for each of the alignments, and a visual inspection of the alignment was made using Insight (*37*).

As another strategy for comparison of the DNA structures, Curves (*38*) was run on all the polyamide−DNA complexes and all the zinc finger−DNA complexes. In addition, Curves also was run on B-DNA (*39*). Comparisons of the output from Curves focused on the width and depth of the major and minor grooves and on base pair parameters such as buckle, shear, propeller twist, opening, and *X* and *Y* displacement. For major and minor groove comparisons, the groove dimensions were taken from (1) the region of the polyamide−DNA complex closest to the polyamide binding site and (2) the region on the zinc finger−DNA complex that was closest to the expected polyamide binding site present in our experiments. The average of the buckle, shear, propeller twist, and opening parameters were taken from the global base−base parameter output of Curves. Parameters for individual base pairs were also compared separately.

RESULTS

Gel mobility shift experiments and DNase I footprinting experiments were used to analyze binding of the zinc finger proteins, binding of polyamides, and interactions between the zinc fingers and the match polyamides that recognized

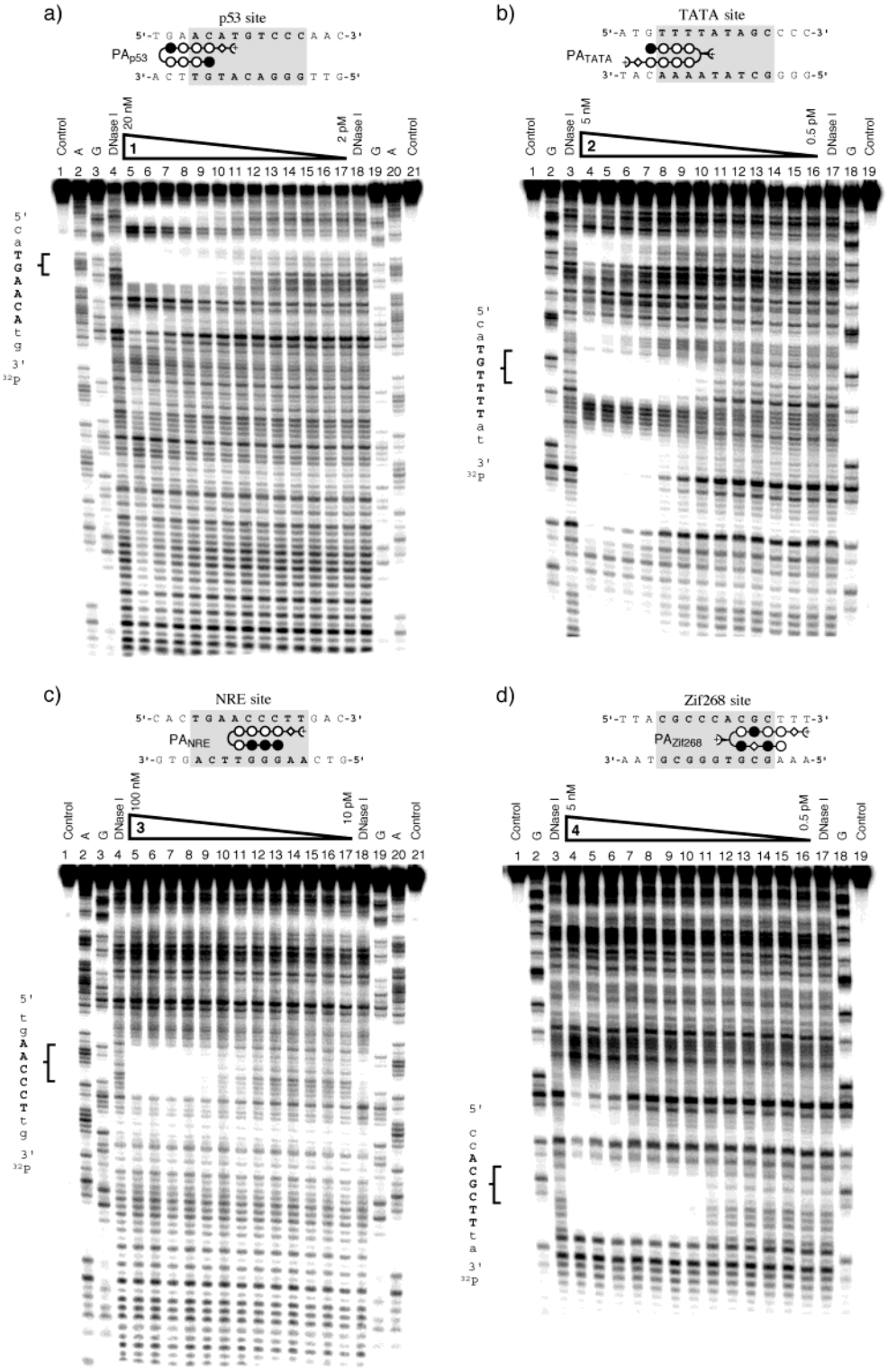

FIGURE 5: Quantitative DNase I footprint titration experiments used to monitor binding of polyamides to the oligonucleotides shown in Figure 4. Oligonucleotides were obtained as *Eco*RI/*Not*I restriction fragments from the pBluescript II SK+ plasmid and were 3′-^{32}P-labeled. Panel a contains PA$_{p53}$ (**1**) on oligonucleotide 1: lanes 1 and 21, intact DNA; lanes 2 and 20, A-specific chemical sequencing reaction; lanes 3 and 19, G-specific chemical sequencing reaction; lanes 4 and 18, DNase I digestion products in the absence of polyamide; lanes 5−17, DNase I digestion products in the presence of 20, 10, 5, 2, 1, 0.5, 0.2, and 0.1 nM and 50, 20, 10, 5, and 2 pM polyamide, respectively. Panel b contains PA$_{TATA}$ (**2**) on oligonucleotide 2: lanes 1 and 19, intact DNA; lanes 2 and 18, G-specific chemical sequencing reaction; lanes 3 and 17, DNase I digestion products in the absence of polyamide; lanes 4−16, DNase I digestion products in the presence of 5, 2, 1, 0.5, 0.2, and 0.1 nM and 50, 20, 10, 5, 2, 1, and 0.5 pM polyamide, respectively. Panel c contains PA$_{NRE}$ (**3**) on oligonucleotide 1: lanes 1 and 21, intact DNA; lanes 2 and 20, A-specific chemical sequencing reaction; lanes 3 and 19, G-specific chemical sequencing reaction; lanes 4 and 18, DNase I digestion products in the absence of polyamide; lanes 5−17, DNase I digestion products in the presence of 100, 50, 20, 10, 5, 2, 1, 0.5, 0.2, and 0.1 nM and 50, 20, and 10 pM polyamide, respectively. Panel d contains PA$_{Zif268}$ (**4**) on oligonucleotide 2: lanes 1 and 19, intact DNA; lanes 2 and 18, G-specific chemical sequencing reaction; lanes 3 and 17, DNase I digestion products in the absence of polyamide; lanes 4−16, DNase I digestion products in the presence of 5, 2, 1, 0.5, 0.2, and 0.1 nM and 50, 20, 10, 5, 2, 1, and 0.5 pM polyamide, respectively.

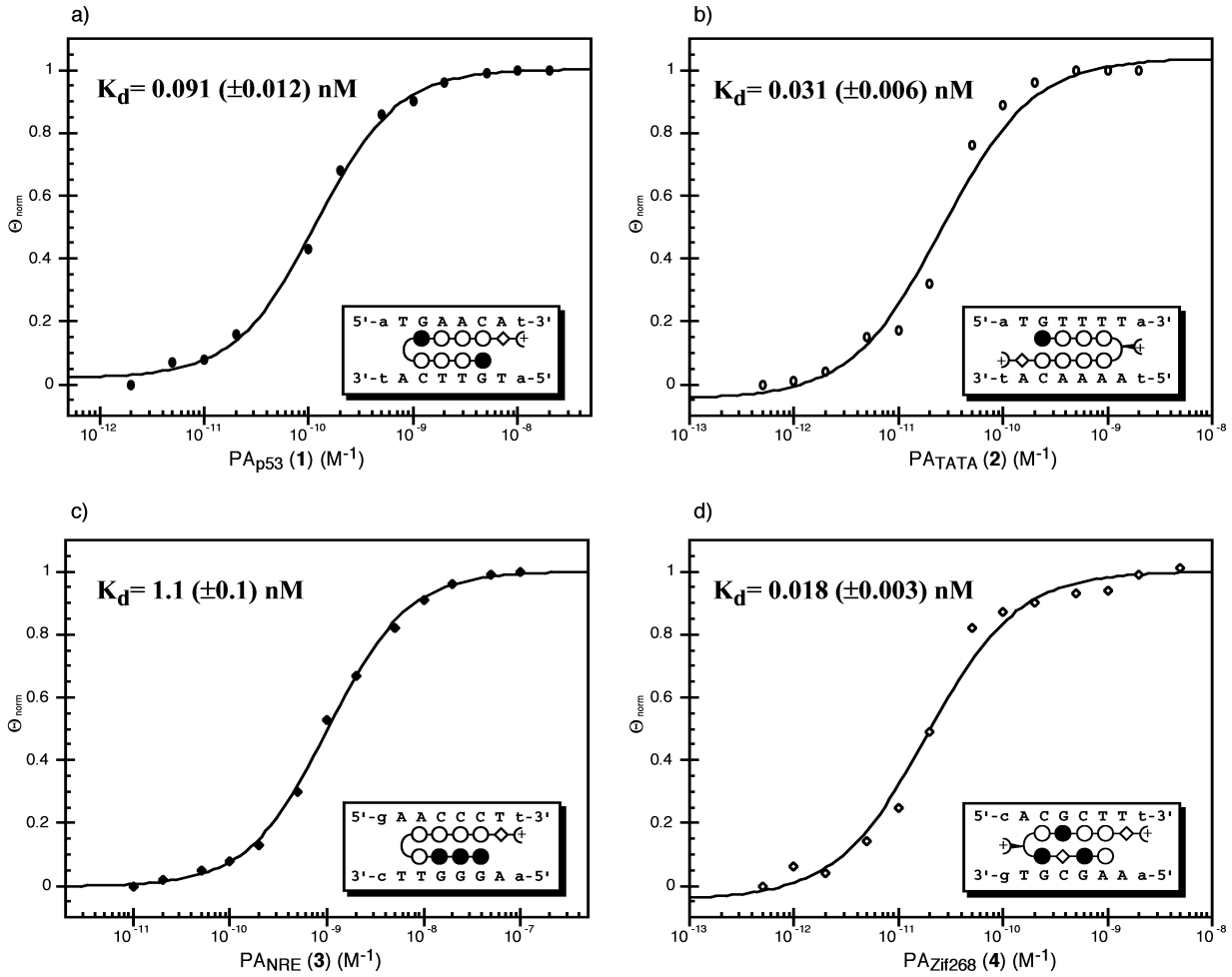

FIGURE 6: Binding isotherms derived from the DNase I quantitative footprint titration experiments (Figure 5) as shown for the PA_{p53} (a), PA_{TATA} (b), PA_{NRE} (c), and PA_{Zif268} (d) polyamides. In each case, isotherms represent binding at the match target site in the minor groove, which has the sequence shown in the lower right panel of the figure and which overlaps with the nine base pair site in the major groove recognized by the corresponding zinc finger protein. Θ_{norm} points were obtained using storage phosphor autoradiography and processed as previously described (*28*). Each data point represents the average of three independent quantitative footprint titration experiments, and the solid curves are the best-fit Langmuir binding titration isotherms obtained from a nonlinear least-squares algorithm where $n = 1$.

overlapping sites. In competition studies, control experiments also were performed with mismatch polyamides to help ensure the specificity of the observed effects. To facilitate comparison of different studies, all experiments were carried out with identical buffer conditions, temperature, equilibration times of the binding reactions, and order of the addition of the components into the reaction mixtures.

Polyamide Equilibrium Dissociation Constants. A set of pyrrole−imidazole polyamides was designed, synthesized, and purified for our competitive binding studies. Structures of these polyamides and their expected modes of binding with the DNA minor groove, as predicted on the basis of "pairing rules" (*4*), are shown in Figures 2 and 3. Polyamides **1**−**4** are referred to as PA_{p53}, PA_{TATA}, PA_{NRE}, and PA_{Zif268} (where our nomenclature indicates which binding site each polyamide has been designed to recognize).

We used quantitative DNase I footprint titration analysis to determine the apparent dissociation constants for the polyamides. Oligonucleotide 1 was used for PA_{p53} and PA_{NRE}; oligonucleotide 2 was used for PA_{TATA} and PA_{Zif268} (Figure 4). The oligonucleotides were labeled from the 3′-end. DNase I footprinting experiments (Figure 5), done at a series of different polyamide concentrations, reveal the location of the binding site for each polyamide and allow determination of the binding constants. These footprinting experiments (Figure 5) show that PA_{TATA} and PA_{Zif268} polyamides also bind specifically to other match and single base pair mismatch sites (as defined by the pairing rules) found on the restriction fragment at the same or higher concentration, respectively. Quantitative analysis of the degree of protection observed at each polyamide concentration allowed us to present the data of the DNase I footprinting experiments as binding isotherms (Figure 6). The apparent K_D, equal to $1/K_A$, was determined from the binding isotherms by fitting the data points with a modified Hill equation, as previously described (*28*). These binding isotherms and apparent dissociation constants for each polyamide represent the average of three independent experiments, and all these polyamides have at least nanomolar affinity for their expected target sites.

Determination of Zinc Finger Dissociation Constants. This study used Zif268 and three variants, specific for the p53, NRE, and TATA binding sites, that had been selected via phage display. (Note that the sequential selection protocol (*9*) used to obtain these variants allowed extensive changes in the recognition site, since six amino acids in each finger had been randomized.) Quantitative gel shift analysis was used to determine the fraction of the DNA fragment bound

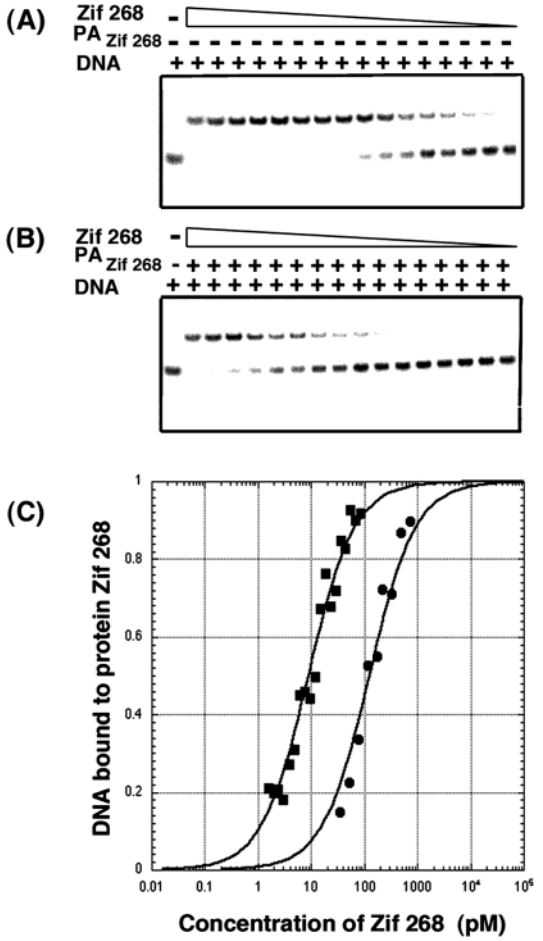

FIGURE 7: Gel mobility shift experiment showing that the PA_{Zif268} polyamide interferes with binding of Zif268 protein. Panel A presents binding of Zif268 protein in the absence of polyamide, where upper band on the gel represents the protein−DNA complex. Protein was diluted 1.5× between lanes, and the 27 bp DNA probe had a concentration of 0.5 pM. Panel B presents a similar binding experiment to that in panel A, but this was performed in the presence of a constant amount of polyamide. The concentration was chosen as $10K_D^{PA}$ and thus is expected to give about 90% saturation of the site in the absence of protein. Panel C presents the Zif268 binding isotherms in the absence (■) and in the presence (●) of PA_{Zif268}. Each data point represents the average of the three independent gel mobility shift experiments. The binding curves show that a protein concentration of 10 pM gives 50% occupancy when no polyamide is present; a protein concentration of 182 pM is required to give 50% occupancy when the polyamide is present.

at a series of protein concentrations (Figure 7), and K_D values were calculated from the slope of Scatchard plots. Corrections were made for the active concentration of each protein, which was estimated using stoichiometric competition experiments.

The sequences of the 27 bp oligonucleotides used in gel mobility shift experiments are boxed in Figure 4. (Note that in this figure the oligonucleotides are shown embedded within larger sites that were later used for DNase I footprinting.) The dissociation constants for the zinc fingers (Table 1) were determined from the average of three independent experiments, and the values are comparable to those previously reported (*9*), even though slightly different buffers were used.

Dissociation Constant of Zinc Finger Protein in the Presence of Specific Polyamides. Binding of the polyamides could not be directly observed in our gel shift experiments,

Table 1: Equilibrium Dissociation Constants and Free Energies of DNA−Zinc Finger Protein Binding in the Absence and in the Presence of Polyamides

polyamide/protein	K_D (nM)[a]
$p53_{ZF}$	0.240 ± 0.018
$PA_{p53}/p53_{ZF}$	3.200 ± 0.283
$TATA_{ZF}$	0.204 ± 0.030
$PA_{TATA}/TATA_{ZF}$	4.320 ± 0.582
NRE_{ZF}	0.101 ± 0.009
PA_{NRE}/NRE_{ZF}	3.520 ± 0.248
Zif268	0.010 ± 0.003
PA_{Zif268}/Zif268	0.182 ± 0.009

[a] The reported equilibrium dissociation constants are apparent for the proteins in the presence of polyamides. All constants are the mean values obtained from three or more gel mobility shift experiments.

but competition studies clearly revealed that the polyamides affected formation, stability or both of the zinc finger−DNA complexes. Two types of competition experiments were done to analyze the effects of polyamides on zinc finger binding.

The first set of experiments used a fixed polyamide concentration that would have given ~90% occupancy of the free DNA site, and gel shift experiments were used to determine the apparent binding constant of the zinc finger proteins under these conditions. These gel shift experiments were essentially identical to those done with the protein alone. The long equilibration time, done for all gel shift experiments, ensured that the apparent binding did not depend on the order of addition of the components. Figure 7 shows one set of gel shift experiments, where the apparent binding constant of Zif268 is determined in the presence and absence of the polyamide that recognizes an overlapping site. Binding isotherms for this reaction are shown in Figure 7C, and similar results were obtained for the other polyamide/zinc finger competitive binding titrations. In every case, the presence of the corresponding polyamide significantly decreases (by 13−35-fold) the apparent affinity of the zinc finger protein for the binding site (Table 1).

Interactions between the polyamides and zinc fingers were also studied in experiments that used fixed zinc finger protein concentrations with variable amounts of polyamide. In each of these experiments, the zinc finger proteins were present at active concentrations equal to 10× their respective dissociation constants, and thus about 90% of the DNA was initially shifted by the proteins. Similar binding reactions with increasing amounts of polyamide were conducted, and after allowing for full equilibration, we monitored the effect of the polyamides on formation of the zinc finger−DNA complexes. Gel shift results obtained with the PA_{Zif268} polyamide and the Zif268 protein (Figure 8A) show that the polyamide interferes with formation or stability of the zinc finger−DNA complex. Similar results were obtained using other zinc finger proteins and polyamides that compete for the same binding sites. Protein bound was calculated as a function of polyamide concentration, each data point representing the average of three independent experiments. Data were fit with the modified Hill equation (*28*), enabling us to estimate "inhibition constants". These represent the polyamide concentrations that give 50% inhibition of formation of the respective protein−DNA complex, and we find that these "inhibition constants" are in the subnanomolar range (Table 2).

Testing for Specificity of Zinc Finger/Polyamide Interference Effects. Several types of experiments were done to test

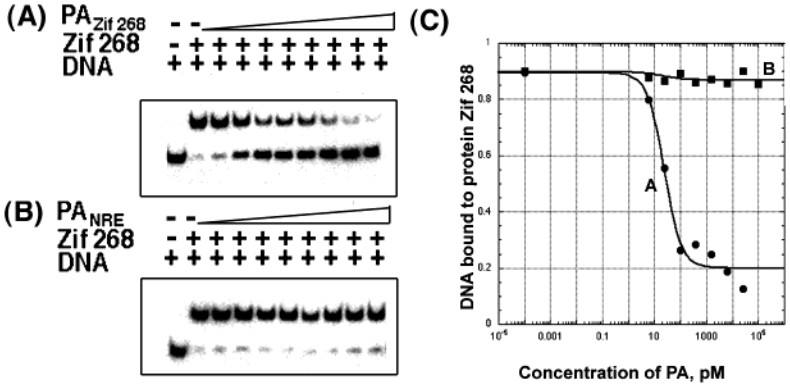

FIGURE 8: Specificity of polyamide interference effects. In these experiments, the active concentration of protein was constant and equal to $10K_D^{prot}$ (giving ~90% of saturation of DNA binding sites when no polyamide was present). The DNA probe was present at 0.5 pM, and the polyamide concentration varies 4-fold between adjacent lanes. Panel A presents representative gel mobility shift results for Zif268 protein binding to DNA probe in the presence of increasing concentrations of PA_{Zif268} polyamide. Panel B presents the corresponding experiments using the Zif268 protein, the Zif268 binding site, and the polyamide PA_{NRE} (note that this polyamide will not bind to the site and thus represents a "mismatch" control for the purposes of this experiment). Panel C presents the effects of polyamides PA_{Zif268} (●) and PA_{NRE} (■) on Zif268 protein binding. Each data point represents the average of three independent experiments, and the difference between these curves emphasizes the specificity of polyamide binding and interference.

Table 2: Equilibrium Inhibition Constants

polyamide/protein	app K_I (nM)[a]
$PA_{p53}/p53_{ZF}$	0.20 ± 0.07
$PA_{TATA}/TATA_{ZF}$	0.04 ± 0.02
PA_{NRE}/NRE_{ZF}	16.40 ± 3.90
$PA_{Zif268}/Zif268$	0.03 ± 0.02

[a] The reported equilibrium inhibition constants are the mean values obtained from three gel mobility shift experiments.

the specificity of the observed interference effects between polyamides and zinc fingers. For example, Figure 8 shows gel shift data obtained with the Zif268 protein−DNA complex. This figure compares the interference effects observed with PA_{Zif268} (the match polyamide with specific binding for this site) and interference effects observed with PA_{NRE} (which is specific for the NRE site and a mismatch polyamide with no binding site on the 27 bp Zif268 oligonucleotide). There is marked interference by PA_{Zif268}, as indicated by the gel shift results in Figure 8A and the sigmodal plot shown in Figure 8C. However, similar concentrations of PA_{NRE} have no measurable effect at this site, as there is no reduction in Zif268 binding even at high polyamide concentrations (Figure 8B,C). Similar data were obtained using other zinc finger/polyamide combinations, and these results show that interference is dependent on having a polyamide that can compete for the same binding site.

Competitive DNase I Footprinting Experiments. Since binding of polyamides could not be directly observed in any of our gel shift experiments, we used DNase I footprinting to further explore the mechanism of polyamide/zinc finger interference effects. In principle, these experiments should allow us to directly monitor polyamide−DNA interactions, zinc finger−DNA interactions, and possible formation of the ternary complex.

Figure 9 shows the results of DNase I footprinting experiments that explored interference effects between the Zif268 protein and the PA_{Zif268} polyamide. These experiments used oligonucleotide 2 (Figure 4), labeled from the 5′ end, to provide a Zif268 protein and PA_{ZF} polyamide binding site. The PA_{NRE} polyamide, which does not have a binding site on this oligonucleotide, was used as a "mismatch" control.

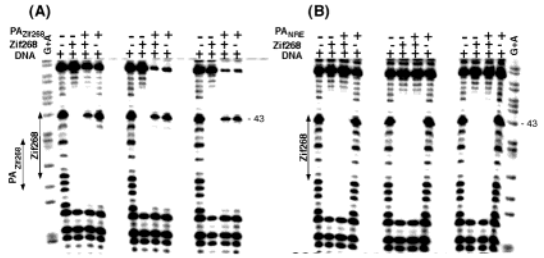

FIGURE 9: DNase I footprinting analysis of polyamide/zinc finger protein interference effects. Panel A presents reactions using Zif268 protein, Zif268 DNA site, and PA_{Zif268} polyamide. The first lane within each group of four has no protein and no polyamide; the second lane has protein but no polyamide; the third lane has protein and polyamide; the forth lane has polyamide alone. When present, the concentration of Zif268 protein was equal to $10K_D$; concentrations of polyamides were 1 nM in the first set of reactions (i.e., the first four lanes), 5 nM in the second set of reactions, and 10 nM in the third set of reactions. Lanes labeled G+A show markers prepared with the Gilbert−Maxam G+A reaction protocol, and binding sites for the Zif268 protein and PA_{Zif268} polyamide are marked on the left side of the gel. Panel B presents the control experiment (with a similar arrangement of lanes and choice of concentration) using the Zif268 protein, Zif268 DNA, and PA_{NRE} polyamide (note that the PA_{NRE} polyamide does not have a binding site on this oligonucleotide and thus serves as a "mismatch" control for these experiments).

Six sets of experiments were performed, using the PA_{Zif268} polyamide at concentrations of 1, 5, and 10 nM (panel A) and then using the PA_{NRE} polyamide at corresponding concentrations (panel B). When the Zif268 protein was present, it was used at a concentration that would have been expected to give approximately 90% occupancy of the free DNA site. As indicated at the top of the respective lanes (Figure 9), four conditions were tested within each set of reactions: (1) the first lane within each set has no protein and no polyamide; (2) the second lane has Zif268 protein but no polyamide; (3) the third lane has Zif268 protein and one of the polyamides; (4) the fourth lane has the same polyamide but contains no protein.

We used Gilbert−Maxam G+A sequencing reactions to determine the precise base positions where cleavage occurred in these footprinting experiments and to locate the binding sites for the Zif268 protein and for the PA_{Zif268} polyamide,

which are marked on the left side of the gels. (Note that experiments in panel B used the PA_{NRE} polyamide, which does not have a binding site on this oligonucleotide.) As expected, there is significant overlap between the region where Zif268 footprints and the region where PA_{Zif268} footprints: the PA_{Zif268} binding site includes bases 32−39, while the Zif268 protein binding site includes bases 35−43 (when counting from the 5′ end). However, it appears that band 43, at the far end of the Zif268 binding site, can only be effectively protected by the protein.

Results obtained with the mismatch polyamide (panel B) are entirely straightforward: Zif268 occupies its binding site in lanes 2 and 3 of each experiment, and the PA_{NRE} polyamide (which is present in lanes 3 and 4 but has no binding site in this oligonucleotide) has no effect on the footprinting patterns. The results with the PA_{Zif268} polyamide (panel A) are somewhat more complicated, but they are the real crux of the experiment. In this panel, lane 2 of each set (protein alone) shows the expected footprint for the Zif268 protein. Lane 4 of each set (polyamide alone) shows the footprints obtained when the PA_{Zif268} polyamide is present at concentrations of 1, 5, and 10 nM. Effects are localized to the expected binding site at low concentration (1 nM), but additional protection due to specific binding of a single base pair mismatch site present in the restriction fragment (near the top of the gel) is seen at higher concentrations.

Obviously, the most interesting results in each set of reactions from panel A involve lane 3, in which both the Zif268 protein and the PA_{Zif268} polyamide were present. At the higher polyamide concentrations (5 and 10 nM), the footprinting patterns obtained with the polyamide/zinc finger combinations (lane 3) appear surprisingly similar to those obtained with the polyamide alone (lane 4). The simplest interpretation of these patterns is that binding of the polyamide displaces the zinc fingers, making the patterns look very similar in lanes 3 and 4. It is somewhat more problematic to explain the pattern obtained in lane 3 of the first set (at a 1 nM concentration of PA_{Zif268}), but this may indicate a mixture of species with the Zif268 protein bound to some fraction of the DNA sites and the PA_{Zif268} polyamide bound to most of the remaining DNA.

Computer Modeling of Polyamide and Zinc Finger Structures. In a further attempt to understand the mechanisms of interference, we examined the structure of various zinc finger−DNA and polyamide−DNA complexes. X-ray crystal structures are now available for the $TATA_{ZF}$ (*34*), $p53_{ZF}$ (*35*), and Zif268 (*6*) zinc finger−DNA complexes. X-ray crystal structures also are available for several polyamide−DNA complexes (*12*, *13*, *15*), and we thought that these structures would be useful for initial modeling, even though the exact sequences of the polyamides and of the binding sites are somewhat different than those used in our current experiments. Our first major conclusion is that we do not see any obvious basis for a steric collision between the zinc fingers and the polyamides. All the polyamide−DNA complexes indicate that these compounds bind exclusively in the minor groove, while the zinc finger−DNA complexes show that these proteins bind in the major groove. [The only exception here involves one lysine (Lys189) in the TATA structure with a high-temperature factor that might reach into the minor groove, but the polyamide binds at the opposite end of this site, far from Lys189.]

Various zinc finger−DNA and polyamide−DNA complexes were superimposed, and these were compared in an attempt to understand the basis for the "negative cooperativity" that we had observed in biochemical studies. Alignments done with the program PROTEUS (*36*) typically used 3−4 sets of phosphates or 3−4 sets of C1′ atoms to superimpose the complexes. The rms deviations in these alignments varied from about 0.6 to about 2 Å, depending on (1) which structures were aligned, (2) which atoms were used for alignment, and (3) how many base pairs were superimposed. However, there were striking and consistent differences in the groove width, and these were large enough that they could readily explain how the polyamides interfere with zinc finger binding. In nearly every alignment that we carried out, the polyamide−DNA complex had a wider and deeper minor groove than that observed in the zinc finger−DNA complexes. There also were a number of cases where superimposing the complexes indicated shifts in the precise arrangement of the base pairs, and these could affect the position of hydrogen bond donors and acceptors that are critical for recognition.

These initial qualitative observations of the structures were confirmed by using the Curves program (*38*) to calculate dimensions of the major and minor grooves. We find that the major grooves in zinc finger−DNA complexes are consistently wider and deeper than the major grooves in the polyamide−DNA complexes. In this set of structures, the Zif268 complex has the deepest major groove (6−8 Å), while the $TATA_{ZF}$ and $p53_{ZF}$ complexes have the widest major grooves (13−14.5 Å). The major groove width of the polyamide−DNA complexes ranged from 9 to 10.5 Å, while the major groove depth ranged from 3 to 5.5 Å. Differences in minor groove width are not quite as consistent when comparing the two classes of complexes, but there is a general tendency for the polyamide−DNA complexes to have wider minor grooves than the zinc finger−DNA complexes.

The initial superimpositions indicated that the orientations of the bases were slightly different in the two types of complexes, and these differences were confirmed and analyzed using the program Curves. In general, we find the following: (1) The two base pairs in the middle of the binding region have negative opening angles in the polyamide−DNA complexes ($-12.22° \pm 5.71°$). No such region is observed in the zinc finger−DNA structures, which on average have more positive opening angles ($1.86° \pm 4.23°$ averaged over the entire binding region of all of the complexes). (2) The zinc finger complexes have a larger negative *X*-displacement of the base pairs than do the polyamide complexes. Averaged over the respective binding sites for each set of complexes, the *X*-displacement values are -1.54 ± 0.28 Å for the zinc finger−DNA complexes and -0.13 ± 0.35 Å for the polyamide−DNA complexes. (3) *X*-displacement parameters for the polyamide−DNA complexes are generally closer to those of B-DNA, whereas opening angles for zinc finger−DNA complexes are generally closer to those of B-DNA. [For a typical B-DNA structure (*39*) averaged over the entire sequence, the values are -0.52 ± 0.25 Å and $-0.31° \pm 5.27°$, respectively.] No significant differences in shear or buckle were noted when comparing the zinc finger and polyamide complexes with those of B-DNA.

DISCUSSION

Compounds that can target specific sites on double-stranded DNA may provide tools for the regulation of gene expression. Excellent progress has been reported in (1) the design and selection of Cys_2His_2 zinc fingers for these purposes (*1*, *2*) and 2) the design of pyrrole−imidazole polyamides that will bind according to well-defined "recognition rules" (*4*). These two broad classes of compounds may provide new reagents for molecular medicine and gene therapy, and recent studies with zinc fingers specifically designed to turn on the VegF gene have shown that such designer transcription factors can work effectively in animal models (*40*).

Our central goal in this paper was to explore how zinc fingers and polyamides might interact when targeted to overlapping recognition sites. We thought this would be interesting from a structural and physical/chemical perspective, and we thought this work also might provide a basis for the eventual development of new regulatory schemes (perhaps where polyamides were used to help regulate the binding of zinc finger proteins or visa versa). Our strategy in these studies was to (1) pick a set of zinc finger proteins that had been carefully characterized, (2) design polyamides that would target sequences that overlap the binding sites of these proteins, and (3) carefully characterize the DNA-binding affinity for each set of compounds under identical buffer conditions. We then used a set of biochemical studies (involving gel mobility shifts and DNase I footprinting experiments) to see what happened when zinc fingers and polyamides that recognized the same DNA site were mixed together.

Our central conclusion from these biochemical studies is that polyamides interfere with the binding of zinc finger proteins when the two compounds recognize overlapping, or partially overlapping, binding sites on the minor and major groove sides of the DNA, respectively. This is clearly demonstrated by interference experiments that use the gel mobility shift assay to monitor zinc finger binding (Figures 7 and 8), and this result holds for every combination of zinc fingers and polyamides that we have tested, when they recognize overlapping or partially overlapping binding sites. It also is clear that this "negative cooperativity" requires direct interactions of the polyamide with the zinc finger binding site: polyamides directed to other DNA sites show no interference with the binding of a given zinc finger protein (as indicated, for example, in the data of Figure 8B).

In an attempt to understand the structural and energetic basis for this "negative cooperativity", we have examined and compared crystal structures that are available for a set of zinc finger−DNA and polyamide−DNA complexes. In every case, structures of the relevant zinc finger−DNA complexes show that the proteins bind in the major groove, while structures of polyamide−DNA complexes show that these compounds bind in the minor groove. There does not appear to be any basis for a van der Waals collision (or any other direct contact) between the protein and the polyamide when they bind to overlapping sites. However, structural comparisons do show striking differences between the DNA conformations in the polyamide−DNA complexes and those in the zinc finger−DNA complexes. Differences in the groove dimensions are quite clear: (1) The minor groove tends to be wider in the polyamide−DNA complexes than in the zinc finger−DNA complexes (Figure 10), while (2) the major groove tends to be wider (and often deeper) in the zinc finger−DNA complexes than in the polyamide−DNA complexes. Quantitative comparison of the DNA structures (using output from the program Curves (*38*)) reveals many other differences between zinc finger−DNA and polyamide−DNA complexes, and many of these differences will affect the precise position and orientation of key hydrogen bond donors and acceptors within the DNA site. At this stage, it seems very plausible that differences in the preferred DNA conformations could explain the "negative cooperativity" that we have observed when zinc fingers and polyamides are targeted to the same site. We assume that (1) the free DNA is somewhat "plastic" and that each compound can induce an appropriate conformation when it binds alone but that (2) simultaneous binding is difficult because the two types of compounds prefer somewhat different DNA conformations. (Note that if the conformational preferences of a given DNA sequence were more rigid, it might be hard to design polyamides for one class of sites and might be hard to design zinc fingers for another class of sites. This does not seem to be the primary problem.) In short, our modeling suggests that negative cooperativity may involve "allosteric" effects of changes in the DNA structure, and considering differences in the relative dimensions of the major and minor groove (Figure 10) makes it easy to picture why these changes may be so important.

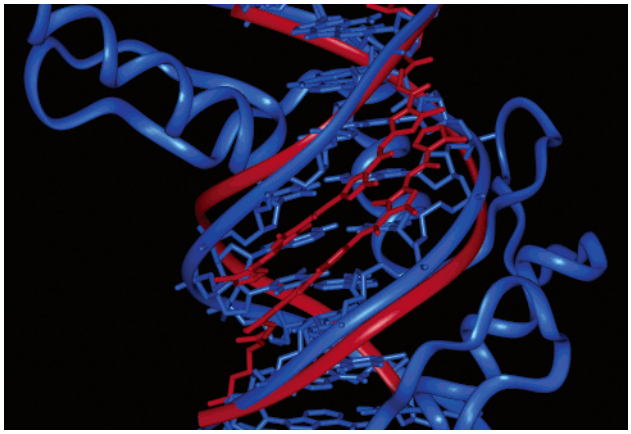

FIGURE 10: Superposition of zinc finger−DNA complex [coordinates are from ref *34*] (blue) and polyamide−DNA complex [coordinates are from ref 13] (red) oriented to highlight differences in minor groove width. Such "allosteric" changes in the groove dimensions may explain the "negative cooperativity" observed in our binding studies with polyamides and zinc fingers.

We undertook this study to investigate how polyamides and zinc fingers interact when they bind to overlapping sites on double-stranded DNA and show here an example of allosteric inhibition of a major-groove binding protein by unmodified polyamides. One could envision that designed zinc finger proteins could be displaced by small molecule polyamides, thereby providing both an on and off switch for gene regulation. Furthermore, phage selection technology may allow for the generation of artificial zinc finger proteins that only bind their target DNA sites with high affinity in the presence of a bound polyamide in the minor groove of the site. The results of this study give key insights into how a zinc finger/polyamide system might be designed to regulate gene expression.

ACKNOWLEDGMENT

$TATA_{ZF}$, NRE_{ZF}, and $p53_{ZF}$ zinc finger peptides were overexpressed, purified, and submitted from Scot A. Wolfe, Robert Grant, and Sandra Fay-Richard, respectively. The pET-21d expression vector transformed in BL21(DE3) was submitted by Bryan S. Wang. We thank Ezra Peisach for a critical reading of this manuscript, and we thank members of the Pabo lab for their support and useful discussions throughout the experimental process and writing of this manuscript.

REFERENCES

1. Pabo, C. O., Peisach, E., and Grant, R. (2003) Design and Selection of Novel Cys2His2 Zinc Finger Proteins, *Annu. Rev. Biochem. 70*, 313−340.
2. Jamieson, A. C., Miller, J. C., and Pabo, C. O. (2003) Drug Discovery with Engineered Zinc Finger Proteins, *Nat. Rev. Drug Discovery 2*, 361−368.
3. Dervan, P. B. (2001) Molecular recognition of DNA by small molecules, *Bioorg. Med. Chem. 9*, 2215−2235.
4. Dervan, P. B., and Edelson, B. S. (1999) Recognition of the DNA minor groove by pyrrole-imidazole polyamides, *Curr. Opin. Struct. Biol. 13*, 284−299.
5. Wolfe, S. A., Nekludova, L., and Pabo, C. O. (2000) DNA Recognition by Cys2His2 Zinc Finger Proteins, *Annu. Rev. Biophys. Biomol. Struct. 29*, 183−212.
6. Elrod-Erickson, M., Rauld, M. A., Nekludova, L., and Pabo, C. O. (1996) Zif268 protein-DNA complex refined at 1.6å: a model system for understanding zinc finger-DNA interactions, *Structure 4*, 1171−1180.
7. Pavletich, N. P., and Pabo, C. O. (1991) Zinc Finger-DNA Recognition: Crystal Structure of a Zif268-DNA Complex at 2.1 Å, *Science 252*, 809−817.
8. Rebar, E. J., and Pabo, C. O. (1994) Zinc Finger Phage: Affinity Selection of Fingers with New DNA-Binding Specificities, *Science 263*, 671−673.
9. Greisman, H. A., and Pabo, C. O. (1997) A General Strategy for Selecting High-Affinity Zinc Finger Proteins for Diverse DNA Target Sites, *Science 275*, 657−661.
10. Choo, Y., and Klug, A. (1994) Selection of DNA Binding Sites for Zinc Fingers Using Rationally Randomized DNA Reveals Coded Interactions, *Proc. Natl. Acad. Sci. U.S.A. 91*, 11168−11172.
11. Segal, D. J., Dreier, B., Beerli, R. R., and Barbas, C. F. (1999) Toward Controlling Gene Expression at Will: Selection and Design of Zinc Finger Domains Recognizing Each of the 5'-GNN-3' DNA Target Sequences, *Proc. Natl. Acad. Sci. U.S.A. 96*, 2758−2763.
12. DeClairac, R. P. L., Geierstanger, B. N., Mrksich, M., Dervan, P. B., and Wemmer, D. E. (1997) NMR Characterization of Hairpin Polyamide Complexes with the Minor Groove of DNA, *J. Am. Chem. Soc. 119*, 7909−7916.
13. Keilkopf, C. L., Baird, E. E., Dervan, P. B., and Rees, D. C. (1998) Structure of a photoactive rhodium complex intercalated into DNA, *Nat. Struct. Biol. 5*, 104−109.
14. Keilkopf, C. L., White, S., Szewczyk, Y. W., Turner, J. M., Baird, E. E., Dervan, P. B., and Rees, D. C. (1998) A Structural Basis for Recognition of A·T and T·A Base Pairs in the Minor Groove of B-DNA, *Science 282*, 111−115.
15. Kielkopf, C. L., Bermer, R. E., White, S., Szewczyk, J. W., Turner, J. M., Baird, E. E., Dervan, P. B., and Rees, D. C. (2000) Structural effects of DNA sequence on T·A recognition by hydroxypyrrole/pyrrole pairs in the minor groove, *J. Mol. Biol. 295*, 557−567.
16. Gottesfeld, J. M., Nealy, L. Traunger, J. W., Baird, E. E., and Dervan, P. B. (1997) Regulation of gene expression by small molecules, *Nature 387*, 202−205.
17. Dickinson, L. A., Gulizia, R. J., Traunger, J. W., Baird, E. E., Mosier, D. E., Gottesfeld, J. M., and Dervan, P. B. (1998) Inhibition of RNA Polymerase II Transcription in Human Cells by Synthetic DNA-Binding Ligands, *Proc. Natl. Acad. Sci. U.S.A. 95*,12890−12895.
18. Sluka, J. P., Horvath, S. J., Glasgow, A. C., Simon, M. I., and Dervan, P. B. (1990) Importance of minor-groove contacts for the recognition of DNA by the binding domain of Hin recombinase, *Biochemistry 29*, 6551−6561.
19. Dickinson, L. A., Trauger, J. W., Baird, E. E., Dervan, P. B., Graves, B. J., and Gottesfeld, J. M. (1999) Inhibition of Ets-1 DNA Binding and Ternary Complex Formation between Ets-1, NF-κB, and DNA by a Designed DNA-binding Ligand, *J. Biol. Chem. 274*, 12765−12773.
20. Nealy, L. Trauger, J. W., Baird, E. E., Dervan, P. B., and Gottesfeld, J. M. (1997) Importance of minor groove binding zinc fingers within the transcription factor IIIA-DNA complex, *J. Mol. Biol. 274*, 439−445.
21. Oakley, M. G., Mrksich, M., and Dervan, P. B. (1992) Evidence that a minor groove-binding peptide and a major groove-binding protein can simultaneously occupy a common site on DNA, *Biochemistry 31*, 10969−10975.
22. Bremer R. E., Baird, E. E., and Dervan, P. B. (1998) Inhibition of major-groove-binding proteins by pyrrole-imidazole polyamides with an Arg-Pro-Arg positive patch, *Chem. Biol. 5*, 119−133.
23. Winston, R. L., Ehley, J. A., Baird, E. E., Dervan, P. B., and Gottesfeld, J. M. (2000) Asymmetric DNA Binding by A Homodimeric bHLH Protein, *Biochemistry 39*, 9092−9098.
24. Wolfe, S. A., Greisman, H. A., Ramm, E. I., and Pabo, C. O. (1999) Analysis of zinc fingers optimized via phage display: evaluating the utility of a recognition code, *J. Mol. Biol. 285*, 1917−1934.
25. Brenowitz, M., Senear, D. F., Shea, M. A., and Ackers, G. K. (1986) Quantitative DNase Footprint Titration - A Method for Studying Protein-DNA Interactions, *Methods Enzymol. 130*, 132−181.
26. Brenowitz, M., Senear, D. F., Shea, M. A., and Ackers, G. K. (1986) "Footprint" Titrations Yield Valid Thermodynamic Isotherms, *Proc. Natl. Acad. Sci. U.S.A. 83*, 8462−8466.
27. Senear, D. F., Brenowitz, M., Shea, M. A., and Ackers, G. K. (1986) Energetics of cooperative protein-DNA interactions: comparison between quantitative deoxyribonuclease footprint titration and filter binding, *Biochemistry 25*, 7344−7354.
28. Trauger, J. W., and Dervan, P. B., (2001) Footprinting methods for analysis of pyrrole-imidazole polyamide/DNA complexes, *Methods Enzymol. 340*, 450−466.
29. Elrod-Erickson, M., and Pabo, C. O. (1999) Binding Studies with Mutants of Zif268. Contribution of Individual Side Chains to Binding Affinity and Specificity in the Zif268 Zinc Finger-DNA Complex, *J. Biol. Chem. 274* (27), 19281−19285.
30. Elrod-Erickson, M., Benson, T. E., and Pabo, C. O. (1998) High-resolution structures of variant Zif268-DNA complexes: implications for understanding zinc finger-DNA recognition, *Structure 6* (4), 451−464.
31. Baird, E. E., and Dervan, P. B. (1996) Solid Phase Synthesis of Polyamides Containing Imidazole and Pyrrole Amino Acids, *J. Am. Chem. Soc. 118*, 6141−6146.
32. Trauger, J. W., Baird, E. E., and Dervan, P. B. (1996) Recognition of DNA by designed ligands at subnanomolar concentrations, *Nature 382*, 559−561.
33. Swalley, S. E., Baird, E. E., and Dervan, P. B. (1996) Recognition of a 5'-(A,T)GGG(A,T)$_2$-3' Sequence in the Minor Groove of DNA by an Eight-Ring Hairpin Polyamide, *J. Am. Chem. Soc. 118*, 8198−8206.
34. Wolfe, S. A., Grant, R., and Pabo, C. O. (2001) Beyond the "Recognition Code": Structures of Two Cys_2His_2 Zinc Finger/TATA Box Complexes, *Structure 9*, 717−723.
35. Grant, R., Richards, S. F., and Pabo, C. O. (2001) Personal communication.
36. Pabo, C. O., and Nekludova, L. (2000) Geometric analysis and comparison of protein-DNA interfaces: why is there no simple code for recognition? *J. Mol. Biol. 301*, 597−624.
37. *MSI*, San Diego, CA.
38. Stofer, E., and Lavery, R. (1994) Measuring the Geometry of DNA Grooves, *Biopolymers 34*, 337−346.
39. Drew, H. R., Wing, R. M., Takano, T., Broka, C., Tanaka, S., Itakura, K., and Dickerson, R. E. Structure of a B-DNA Dodecamer: Conformation and Dynamics, *Proc. Natl. Acad. Sci. U.S.A. 78*, 2179−2183.
40. Rebar, E. J., Huang, Y., Hickey, R., Nath, A. K., Meoli, D., Nath, S., Chen, B., Xu, L., Liang, Y., Jamieson, A. C., Zhang, L., Spratt, S. K., Case, C. C., Wolffe, A., Giordano, F. J. (2002) Induction of angiogenesis in a mouse model using engineered transcription factors, *Nat. Med. 8*, 1427−1432.

BI030223C